Journal of Applied Polymer Science

Aminating modification of viscose fibers and their CO_2 adsorption properties

Qinghua Wu,[1] Shuixia Chen,[1,2] Shihe Luo,[1] Teng Xu[1]

[1]Key Laboratory for Polymeric Composite & Functional Materials of Ministry of Education, School of Chemistry and Chemical Engineering, Sun Yat-Sen University, Guangzhou 510275, People's Republic of China

[2]Materials Science Institute, Sun Yat-Sen University, Guangzhou 510275, People's Republic of China

Correspondence to: S. Chen (E-mail: cescsx@mail.sysu.edu.cn)

ABSTRACT: An adsorbent for CO_2 capture was prepared by the grafting of acrylonitrile (AN) onto viscose fibers (VFs); this was followed by amination with triethylene tetramine (TETA). The effects of the reaction conditions, such as the concentrations of the monomer, initiator, and nitric acid, on the grafting degree and grafting efficiency were studied. The adsorption performance of the adsorbent for CO_2 was evaluated by fixed-bed adsorption. The highest dynamic adsorption capacity of the adsorbent for CO_2 was 4.35 mmol/g when the amine content of the adsorbent VF–AN–TETA reached 13.21 mmol/g. Compared with the polypropylene (PP)-fiber-based adsorbent (PP–AN–TETA), VF–AN–TETA with hydroxyl groups on the fibers facilitated the diffusion of CO_2 and water and led to a higher CO_2 adsorption capacity than that of PP–AN–TETA. The VF–AN–TETA adsorbent also showed good regeneration performance: its CO_2 adsorption capacity could still retain almost the same capacity as the fresh adsorbent after 10 adsorption–desorption cycles. © 2015 Wiley Periodicals, Inc. J. Appl. Polym. Sci. **2016**, *133*, 42840.

KEYWORDS: adsorption; fibers; functionalization of polymers; grafting; surfaces and interfaces

Received 3 May 2015; accepted 16 August 2015

DOI: 10.1002/app.42840

INTRODUCTION

Considerable attention has been paid to reducing greenhouse gas emissions, especially for the capture and storage of CO_2, mainly resulting from fossil fuel combustion. There are several methods being developed for CO_2 capture and storage, including cryogenic distillation, solution absorption, and adsorption by solid adsorbents and membrane separation.[1] Among these available approaches, adsorption by solid adsorbents could be used as a promising method for capture of CO_2. Various well-known adsorbents, such as activated carbon,[2] carbon nanotubes,[3] zeolites, silica gel,[4,5] mesoporous silica,[5,6] metal–organic frameworks,[6–8] and amine-functionalized[9] adsorbents, have been reported. Compared with liquid amines,[10,11] solid adsorbents can prevent the viscosity, excessive corrosion problems, and foaming issues that are caused by liquid amines.

A class of amine-functionalized adsorbents with porous silica, especially mesoporous silica materials as substrates, were proven to be good solid adsorbents for CO_2 capture. A variety of mesoporous silica materials, such as SBA-15,[12] MCM-41,[13] and hollow mesoporous silica (HMS),[14] were evaluated. Unlike zeolites, activated carbon, or metal–organic frameworks, these amine-modified fibers are able to retain good adsorption capacities even in the presence of water and can be regenerated under mild conditions.[15] However, the adsorption capacity for CO_2 mainly depends on the amine loading and the pore volume of the material. Increasing the amine loading on a mesoporous silica substrate may lead to a reduction in the CO_2 adsorption capacity because the material will agglomerate when the amine content increases to a certain amount; this can block the pores and then hinder contact between the amine groups and CO_2 molecules and, thus, limit the further development of mesoporous silica materials.[16,17] So, there has been a tendency to develop alternative substrates to improve the amine capacity without effects on the adsorption performance.

Compared with mesoporous silica particles, fibrous material is a promising adsorbent substrate as well, which possesses large external surface area, short transit distance, low pressure drops, and well flexibility. In addition, grafting has little influence on the surface area of fibers and can effectively improve the adsorption capacity for CO_2 even with a high grafting degree (G; wt %). Meanwhile, grafted fibers also have a high chemical stability, which is helpful for reuse. Hence, a solid amine fibrous adsorbent is a promising material for CO_2 capture.

Here, viscose fibers (VFs) with unique advantages, such as a large number of hydroxyl groups and hydrophilicity, were employed as a substrate for the preparation of a novel kind of solid amine fibers. VFs were grafted with acrylonitrile (AN) and then aminated by triethylene tetramine (TETA) to introduce amine groups. The objective of this study was to explore the CO_2 adsorption capacity of this

novel adsorbent. The physicochemical and regeneration properties of the material were investigated, and the effects, such as the content of amine groups, CO_2 concentration of the flow, and temperature on CO_2 adsorption, were probed.

EXPERIMENTAL

Materials

All of the reagents used in this research were analytical grade. The VFs (degree of polymerization = 600–750, fineness = 1.67 dtex, length = 38 mm) used for this study were manufactured by Jilin Chemical Fiber Group Co., Ltd. AN was used after distillation for the removal of the inhibitor. Ceric ammonium nitrate [CAN; $Ce(NH_4)_2(NO_3)_6$], TETA, aluminum chloride hydrate, and nitric acid (HNO_3) were used as received.

Preparation of the Solid Amine Fibrous Adsorbents (Scheme 1)

Grafting of AN onto the VFs. For a typical reaction, VFs were soaked in a 4 wt % sodium hydroxide solution (with a liquor ratio of the fibers to the solution of 1:50.) for 24 h; this was followed by immersion in acetone overnight and finally washing with distilled water and drying at 60°C. Then, 1.0 g of NaOH-treated VFs was immersed into a 50-mL CAN aqueous solution with a concentration of 50 mmol/L at 30°C for 1 h. A mixed solution containing 6 mL of 1.0 mol/L HNO_3 and 51.3 mL of distilled water was added to a 100-mL, three-necked flask, into which nitrogen was purged for 30 min to eliminate oxygen. Then, 1.0 g of VFs, which were soaked with CAN solution, was added and stirred for 10 min; this was followed by the addition of 2.7 mL of AN. The grafting reaction was carried out at 50°C for 1 h in an N_2 atmosphere. After the grafting reaction, the grafted fibers (VF–AN) were extracted in a Soxhlet apparatus with methanol for 48 h to remove the residual monomer and homopolymer (polyacrylonitrile). The obtained product, VF–AN, was dried *in vacuo* at 60°C for 24 h.

Amination of VF–AN. The procedures of the amination reaction of VF–AN were as follows: 1.0 g of VF–AN fibers, 70 mL of TETA, and 0.7 g of aluminum chloride hydrate were added to a 100-mL flask and stirred. The reaction was carried out at 130°C for 5 h. Then, the aminated fiber (VF–AN–TETA) was washed successively with distilled water and ethyl alcohol and then dried at 60°C *in vacuo* for 5 h. G (wt %) and the grafting efficiency (Ge; wt %) were calculated according to eqs. (1) and (2). The amination degree (Da) presented in molar percentages was calculated according to the formulas in eq. (3):

$$G\,(\text{wt }\%) = \frac{W_g - W_o}{W_o} \times 100\% \quad (1)$$

$$Ge\,(\text{wt }\%) = \frac{W_g - W_o}{m} \times 100\% \quad (2)$$

$$Da\,(\text{mol }\%) = \frac{n_{\text{TETA}}}{n_{\text{AN}}} = \frac{{}^{(W_b - W_a)}/_{146}}{{}^{W_a \times G}/_{(G+1)\times 53}} = \frac{53\times(W_b - W_a)(G+1)}{146\times W_a G} \times 100\% \quad (3)$$

where W_o, W_g, and W_b are the weights of the original, grafted, and aminated fibers, respectively; W_a is the weight of the grafted fibers used for amination; m is the mass of AN; and 146 and 53 are the molar masses of TETA and AN, respectively. n_{TETA} and n_{AN} are the molar quantities of TETA and AN, respectively.

Physical and Chemical Characterization

IR spectra were obtained with a Fourier transform infrared (FTIR) analyzer (Tensor-27, Germany) equipped with a continuum microscope and an attenuated total reflection (ATR) objective. ATR–FTIR measurements were carried out in the range 600–4000 cm^{-1}.

Elemental analysis was used to determine the composition of the fibers. The nitrogen, hydrogen, and carbon content of the fiber samples were determined by a PerkinElmer Vario EL elemental analyzer (Germany).

The adsorption–desorption isotherms of nitrogen at 77.35 K were measured with an automatic gas adsorption instrument (ASAP2020, Micromeritics Corp.) in a relative pressure range from 10^{-6} to 1 after the treated sample was degassed at 150°C. The total pore volume was calculated on the basis of the nitrogen amount adsorbed at relative pressure $P/P_0 = 0.95$. S_{BET} was calculated through the Brunauer–Emmett–Teller method.

A fabric moisture transmission instrument was used to measure the hygroscopic rate of the samples.

CO_2 Adsorption

Breakthrough curves were used to characterize the CO_2 adsorption performances of all of the samples. A fiber sample weighing approximately 1.00 g was packed into a sample tube, into which a dry nitrogen flow was introduced at a flow rate of 33 mL/min for 1 h to remove the air and moisture in the tube. Then, the CO_2/N_2 gas mixture was introduced through the tube at a flow rate of 33 mL/min. The flow rate of the gas was controlled by electronic flow control instruments. The concentration of CO_2 in the influent gas (C_{in}) and effluent (C_{eff}) were analyzed at regular time intervals with a Techcomp 7900 gas chromatograph. After adsorption, a pure nitrogen gas was introduced through the tube at 90°C for the regeneration of spent fibers.

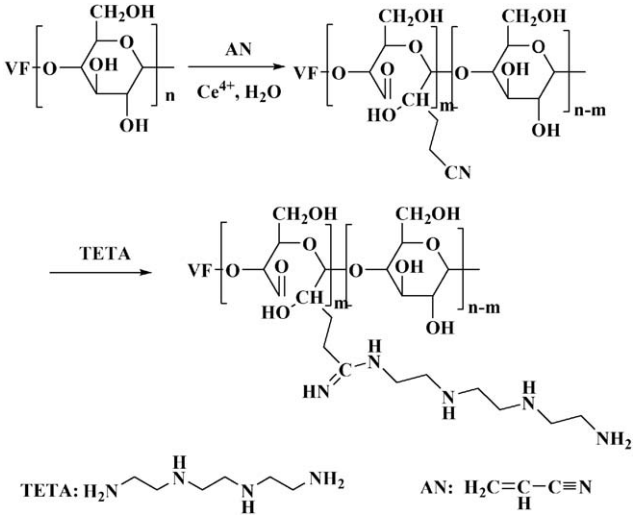

Scheme 1. Synthesis processes for VF–AN–TETA.

RESULTS AND DISCUSSION

Effects of the Reaction Conditions on G and Ge of VF–AN

Effect of the Monomer Concentration. Using certain concentration of Ceric ammonium nitrate (C_{CAN}) and nitric acid (C_{HNO_3}) as

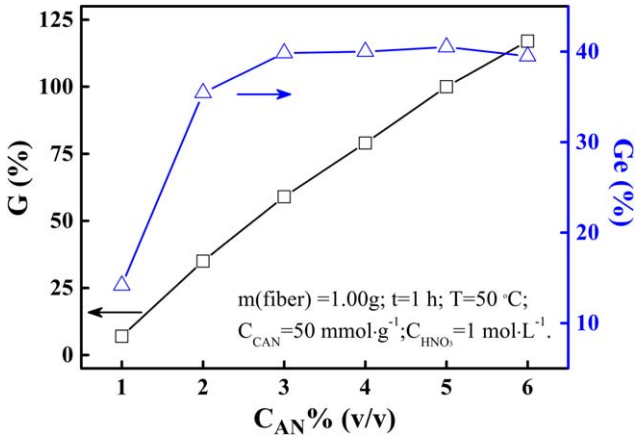

Figure 1. Influence of the AN concentration on *G* and *Ge*. [Color figure can be viewed in the online issue, which is available at wileyonlinelibrary.com.]

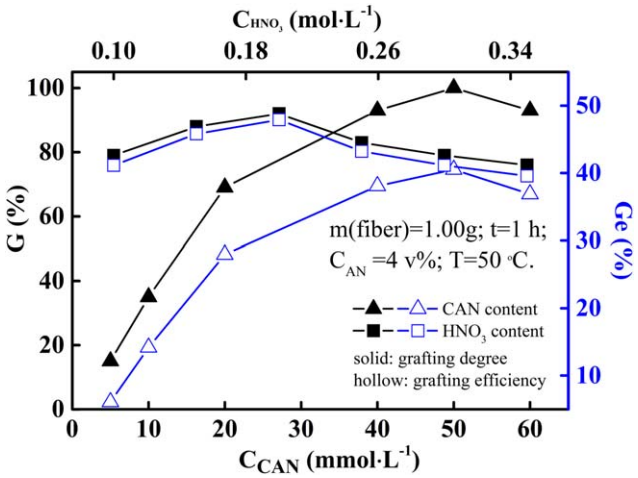

Figure 2. Influence of the initiator and HNO_3 concentrations on *G* and *Ge*. [Color figure can be viewed in the online issue, which is available at wileyonlinelibrary.com.]

the initiator, certain mass of fiber (m(fiber)) was grafted with the monomer AN (C_{AN}) at a specific temperature (T) for specific time (t). The reaction conditions are discussed as fellows. Figure 1 shows the effect of the monomer concentration (AN) on *G* and *Ge* of the VFs pretreated with 4 wt % NaOH. We observed that *G* showed a rising trend, whereas the monomer concentration was in the range 1–6 vol %. The higher the monomer concentration was, the larger the density of the monomer molecules was in the whole grafting system; this led to a greater chance for the reactive collision between the reactive sites of VFs and the monomer molecules and thus an increased *G*. However, the influence of the AN concentration on *G* was significantly different from *Ge*. *Ge* gradually increased with the concentration of AN in the range 1–3 vol %. When the concentration was 3 vol %, the *Ge* value approached its maximum efficiency, 40%; the *Ge* value remained steady when the concentration increased further from 3 to 6 vol %. This result was attributed to the homopolymerization of the monomers; this was an inevitable side reaction, and the probability of its occurrence increased to a great level with increasing monomer concentration. This depleted both the amount of monomer molecules and active sites of VFs during the grafting process and even decreased the monomer diffusion rate; this resulted from the increased viscosity of the entire system. The main factor of homopolymerization led to the decline of contact probability between monomers and active sites. With *G*, *Ge*, and the postprocessing of the removal of the homopolymer from VF–AN, a 5 vol % monomer concentration was chosen for the grafting of AN onto the VFs in the study.

Effect of the CAN Concentration. The effect of the initiator (CAN) concentration on *G* and *Ge* is represented in Figure 2. We observed clearly from the results that with increasing CAN concentration, both *G* and *Ge* increased at first and then decreased gradually. The maximum values of *G* and *Ge* were 100 and 40%, respectively, around a 50 mmol/L concentration of the initiator. This behavior could be reasonably explained as follows: the number of free-radical sites on the VF backbone, onto which AN could be grafted, rose as the initiator concentration increased. However, when the concentration exceeded 50 mmol/L, excessive radicals triggered multiple coupling; this made the homopolymerization of AN become the dominant reaction. Finally, the homopolymer in the product increased dramatically, so the viscosity of the whole reactive system may have increased, and this hindered the diffusion of monomers to active sites, along with cage effect occurrence.

Effect of the HNO_3 Concentration. Figure 2 also depicts the effect of the HNO_3 concentration on *G* and *Ge*. It shows that *G* and *Ge* increased with increasing HNO_3 concentration up to 0.2 mol/L and then decreased while the HNO_3 concentration varied from 0.2 to 0.35 mol/L. This could be explained by the fact that ceric ions reacted in water in the following manner:

$$Ce^{4+} + 3H_2O \rightarrow [Ce(OH)_3]^{3+} + 3H^+ \quad (4)$$

$$2[Ce(OH)3]^{3+} \rightarrow [Ce\text{-}O\text{-}Ce]^{6+} + 3H_2O \quad (5)$$

As $[H^+]$ increased, the equilibria, eqs. (4) and (5), shifted toward the formation of more and more $[Ce]^{4+}$ and $[Ce(OH)_3]^{3+}$. These species, at higher concentrations of acid, played a disadvantageous role in the propagation of the polymeric chain; this lowered *G* and *Ge*. In addition, the chain growth could also have been terminated by the oxidative reaction of ceric ions, as shown in eq. (6):[18–20]

$$Ce^{4+} + H{-}M_n^{\bullet} \rightarrow Ce^{3+} + M_n + H^+ \quad (6)$$

On the other hand, the number of radicals decreased because the decomposition of Ce^{4+}–VF became difficult at HNO_3 concentrations of 0.2 mol/L or even higher.

Chemical Structure and Morphology of the Modified Fibers

The chemical structures of the modified fibers were characterized by ATR–FTIR spectroscopy. The FTIR spectra of the VFs, VF–AN, and VF–AN–TETA are compared in Figure 3. Compared with the spectrum of the VFs, the spectrum of VF–AN showed a weak peak at 1705 cm^{-1}, which corresponded to —C═O group stretching, and a characteristic peak at 2238 cm^{-1} appeared due to —C≡N group stretching. This suggested that AN was successfully grafted onto the surface of the VFs. In the spectrum of VF–AN–TETA, a new peak at 1607 cm^{-1} and a broad band positioned between 3000 and 3500 cm^{-1}, which corresponded to —C═N—[21] and N—H vibrations, indicated that amine groups were introduced onto the VF–AN–TETA fibers.

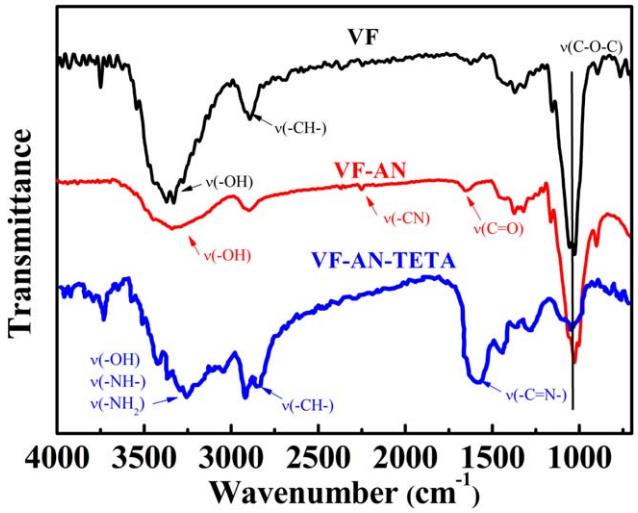

Figure 3. FTIR spectra of the VF and modified fibers. [Color figure can be viewed in the online issue, which is available at wileyonlinelibrary.com.]

In addition, the absorption peak of —C≡N disappeared, along with the appearance of N—H vibrations and the increase of C—H; this proved that TETA had combined with —CN on the surface of the VF–AN fibers.

Effect of the Moisture on the Adsorption of VF–AN–TETA for CO_2

It was meaningful to investigate the effect of moisture on the adsorption of VF–AN–TETA for CO_2 because moisture existed in both the biogas and flue gas. Figure 4 presents the adsorption breakthrough curves of VF–AN–TETA for CO_2 adsorption in the presence or absence of moisture. It was apparent that the adsorption performance of VF–AN–TETA was very different in the two cases. In the absence of moisture, the adsorption capacity for CO_2 was as low as 0.13 mmol/g, and CO_2 completely broke through in less than 6 min. However, in the presence of moisture, the fiber adsorbed all of the CO_2 from the effluent in the initial 8 min, and then, CO_2 completely broke through in the next 20 min. The CO_2 adsorption capacity reached 4.35 mmol/g in the presence of moisture. The results indicate that H_2O participated in the reaction between the CO_2 and amine groups of the adsorbent [eqs. (7) and (8)] and had a substantial promoting effect on CO_2 adsorption.[22–24] As shown in the following equations, in the presence of moisture, 1 mol of RNH_2 or R_1R_2NH (Where R, R_1 and R_2 are alkyl groups.) could adsorb 1 mol of CO_2 to form bicarbonate [eqs. (7) and (8)], whereas 1 mol of RNH_2 or R_1R_2NH could only adsorb 0.5 mol of CO_2 to form carbamate in the absence of H_2O [eqs. (9) and (10)]:

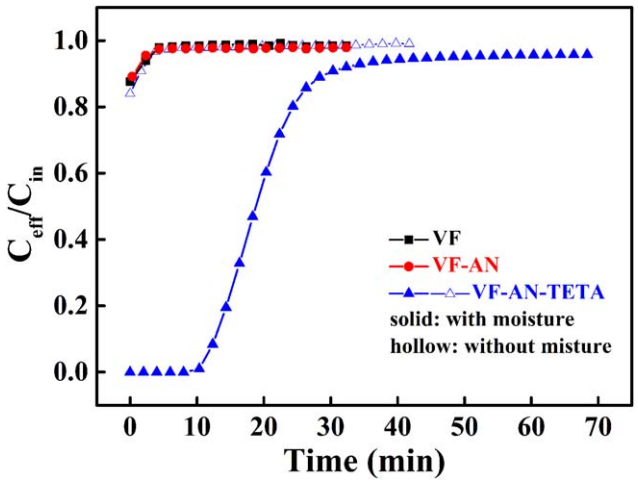

Figure 4. Effect of moisture and functional groups on the adsorption of CO_2 onto the fiber adsorbent (adsorption temperature = 30°C, N_2 = 24 mL/min, CO_2 = 6 mL/min). [Color figure can be viewed in the online issue, which is available at wileyonlinelibrary.com.]

$$CO_2 + RNH_2 + H_2O \rightleftharpoons RNH_3^+ + HCO_3^- \quad (7)$$

$$CO_2 + R_1R_2NH + H_2O \rightleftharpoons R_1R_2NH_2^+ + HCO_3^- \quad (8)$$

$$CO_2 + 2RNH_2 \rightleftharpoons RNH_3^+ + RNHCOO^- \quad (9)$$

$$CO_2 + 2R_1R_2NH \rightleftharpoons R_1R_2NH_2^+ + R_1R_2NCOO^- \quad (10)$$

In comparison with the reference data[15] of some amine-functionalized mesoporous silicas, such as MCM-41 or SBA-15-supported or grafted amine; the CO_2 adsorption capacities were usually in the range of 0.5–3.5 mmol/g.[15] The solid amine VF–AN–TETA fiber in this study achieved a higher adsorption capacity.

Effect of the Functional Group of the Fibers on Its CO_2 Adsorption

To investigate the influence of the nitrogen-containing group on the adsorption, CO_2 adsorption experiments with VF–AN and VF–AN–TETA were carried out to study the influence of functional groups on its adsorption performance. Although the content of nitrogen was 13.47% on VF–AN (Table I), the breakthrough curve of VF–AN revealed that cyano could scarcely capture CO_2, as shown in Figure 4. However, a small amount of CO_2 was still captured by VF–AN; this might have been due to affinity generated by physical adsorption. Comparatively speaking, VF–AN–TETA with a slightly higher nitrogen content adsorbed CO_2 with an adsorption capacity of 4.35 mmol/g. The porosity characterization results indicate that the VF–AN–TETA prepared in this study had a very low porosity (with a Brunauer–Emmett–Teller surface of 7.8 m^2/g and a pore volume of 0.000135 cm^3/g); this meant that the amount of physical adsorption was very small. Most of the adsorption amount was due to the chemisorption by amine groups. The result also indicates that not all of the nitrogen could adsorb CO_2 through chemisorption but that it depended on its chemical environment. It also means that the solid amine fibers could present excellent adsorption performances only in the case of coexistence of the moisture and amines.

Table I. Elemental Analyses of VF, VF–AN, and VF–AN–TETA

	Elemental content (%)			Amine group (mmol/g)	
Fiber	C	H	N	—NH	—NH_2
VF	41.13	6.837	0.00		
VF-AN (*G* = 100%)	54.47	6.242	13.47		
VF-AN-TETA (*Da* = 69.1%)	49.63	8.574	17.17	7.36	2.45

Table II. CO_2 Adsorption Properties of PP–AN–TETA and VF–AN–TETA

	Amine content (mmol/g of fiber)	CO_2 adsorption capacity (mmol/g of fiber)	Amine utilization (%)
VF-AN-TETA	7.78	2.87	36.89
PP-AN-TETA	7.98	1.69	21.18

Effect of the Surface Chemical Structure of the Fiber on Its CO_2 Adsorption

In this study, another aminated fiber (PP–AN–TETA, where PP indicates polypropylene), with PP fiber as a parent fiber, was prepared (according to the preparation method of PP–AN reported in ref. 25) to explore whether the chemical structure of the substrate impacted on CO_2 adsorption. Meanwhile, its CO_2 adsorption behavior was compared with that of VF–AN–TETA, and the corresponding results are presented in Table II and Figure 5. We concluded from Figure 5 that the adsorption performance of VF–AN–TETA was obviously superior to that of PP–AN–TETA; the CO_2 concentration in the effluent gas remained zero for more than 10 min, but PP–AN–TETA tended to break through at the beginning of the adsorption. In addition, the results in Figure 5 also show that it took more time for PP–AN–TETA than VF–AN–TETA to achieve adsorption equilibrium, even though their amine contents were very close (7.98 mmol/g for PP–AN–TETA and 7.78 mmol/g for VF–AN–TETA, as shown in Table II). Anyway, both the adsorption capacity and the amine utilization of PP–AN–TETA were lower than those of VF–AN–TETA under the same conditions (Table II). The main different adsorptive behaviors between VF–AN–TETA and PP–AN–TETA could be explained as follows. On the one hand, the facts show that water itself was favorable for CO_2 adsorption for solid amine fibers, so we deduced that the more hydrophilic the adsorbent was, the better the adsorption performance it had. Fortunately, the results shown in Table III confirmed this deduction. Obviously, the hygroscopic rate of VF–AN–TETA (21.41%) was higher than that of PP–AN–TETA (16.31%), although the cyano group and amino group contents of both adsorbents were similar to each other. In other words, the hydrophilicity of PP–AN–TETA was inferior to that of VF–AN–TETA, and this was attributed to its substrate (VFs), which contained a great number of hydroxyls on its surface. On the other hand, hydroxyls and water can form hydrogen bonds; this fixed water and then accelerated the diffusion of CO_2 on the surface of the adsorbent. Therefore, VF–AN–TETA showed a much better adsorption performance than PP–AN–TETA.

Table III. Hygroscopic Rate of the Parent and Modified Fibers

	Hygroscopic rate (%)		Hygroscopic rate (%)
VF	11.90	PP	0.077
VF-AN (G = 25%)	10.61	PP-AN (G = 25%)	0.11
VF-AN-TETA (Da = 42.7%)	21.41	PP-AN-TETA (Da = 49.9%)	16.31

From what we discussed previously, the chemical structure of the substrate indeed influenced the adsorption performance of the adsorbent. The results also indicates that the solid amine fibers presented excellent adsorption performance only in the case of the coexistence of the moisture and amines. In particular, the hydrophilic solid amine fibers are more suitable for actual application, as CO_2 adsorptions are usually carried out under moist conditions.

Effect of the Amine Density of the Adsorbent on Its CO_2 Adsorption

The influence of the amine density of the VF–AN–TETA fibers on the adsorption capacity was examined. As shown in Figure 6, the dynamic adsorption capacity of VF–AN–TETA increased with increasing amine density of VF–AN–TETA; this was attributed to

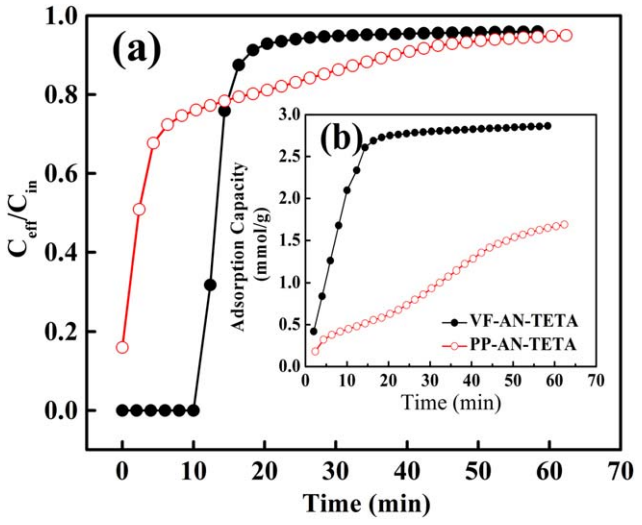

Figure 5. (a) Breakthrough curves of the CO_2 adsorption onto PP–AN–TETA and VF–AN–TETA. (b) Dynamic adsorption capacity (adsorption temperature = 30°C, N_2 = 27 mL/min, CO_2 = 3 mL/min). [Color figure can be viewed in the online issue, which is available at wileyonlinelibrary.com.]

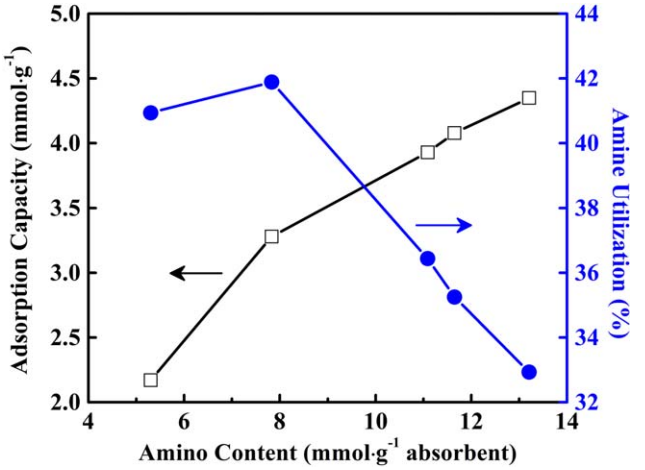

Figure 6. Dynamic adsorption capacity and amine utilization of the VF–AN–TETA fibers with different amino contents (adsorption temperature = 30°C, N_2 = 27 mL/min, CO_2 = 3 mL/min). [Color figure can be viewed in the online issue, which is available at wileyonlinelibrary.com.]

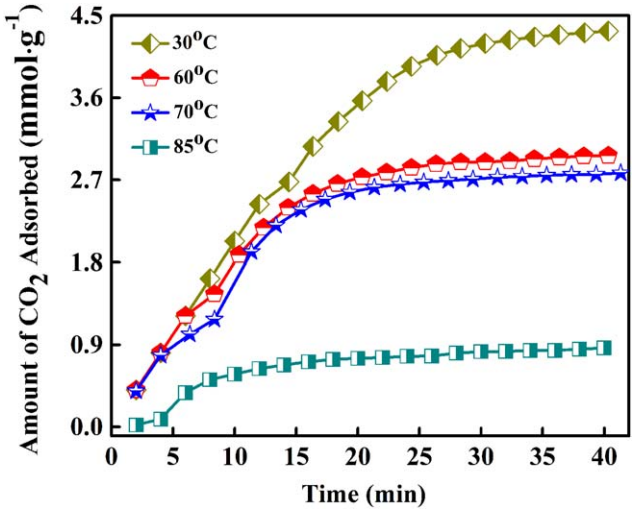

Figure 7. Plot of the amount of CO_2 adsorption versus the adsorption time at various temperatures (fiber mass = 1.0 g, N_2 = 27 mL/min, CO_2 = 3 mL/min). [Color figure can be viewed in the online issue, which is available at wileyonlinelibrary.com.]

the growing amount of reaction sites for CO_2. The amount of CO_2 adsorbed on VF–AN–TETA increased from 2.17 to 4.35 mmol/g with increasing amino content from 5.30 to 13.21 mmol/g. Hence, under the same adsorption conditions, adsorbents with a higher amine density adsorbed more CO_2.

Nevertheless, amine utilization did not increase with the amino content of the adsorbent as the dynamic adsorption capacity did. As shown in Figure 6, after a peak value around 8 mmol/g of amine content was reached, the amine utilization decreased rapidly. All of the grafted TETA was located on the external surface. With increasing *G* of TETA, the thickness of the grafting layer increased accordingly. Apparently, a higher amine content may have resulted in a stronger mass transfer resistance of CO_2 into the inner part of the grafting layer. Consequently, not all of the amine groups in the inner part could contact and react with CO_2; this led to a decrease in the amine utilization.

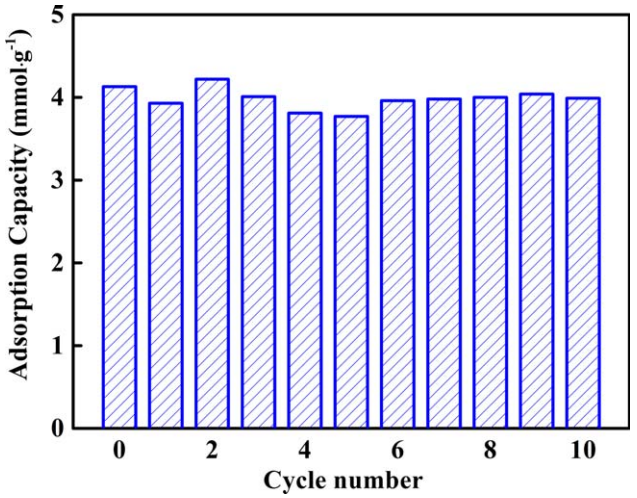

Figure 8. CO_2 adsorption capacity of VF–AN–TETA in 10 adsorption–desorption cycles (fiber mass = 1.0 g, adsorption temperature = 30°C, N_2 = 27 mL/min, CO_2 = 3 mL/min, desorption temperature = 90°C, N_2 = 30 mL/min). [Color figure can be viewed in the online issue, which is available at wileyonlinelibrary.com.]

Effect of the Adsorption Temperature and Regeneration of the Adsorbent

The influence of the temperature on the CO_2 adsorption on VF–AN–TETA was examined, and the amount of CO_2 adsorbed as a function of time is shown in Figure 7. A higher temperature led to a faster diffusion of CO_2 on the surface of VF–AN–TETA. Therefore, it took less time to achieve adsorption equilibrium at a higher temperature. Nevertheless, at higher temperatures, the adsorption capacities were less than those at lower temperatures because of exothermic reactions, such as those in PEI-modified materials.[26,27]

Table IV shows the influence of the temperature on the adsorption capacity and amine utilization of VF–AN–TETA. It was evident that the optimum adsorption capacity (4.30 mmol/g adsorbent) and amine utilization (36.53%) were achieved at 30°C. However, with the elevation of the environmental temperature, both of them decreased obviously: at 85°C, the adsorption capacity decreased to 0.92 mmol/g. We believe that this phenomenon was partly related to the moisture, which played a key role in the process of CO_2 adsorption. As the temperature was elevated, water in the grafting layer evaporated, and hence, the swollen fiber shrank to a compact state. Consequently, the mass transfer resistance of CO_2 grew; this probably hindered the amine group from contacting CO_2. On the other hand, the reaction of TETA and CO_2 was exothermic, and an increase in the temperature facilitated the desorption of CO_2 from the adsorbent rather than adsorption. In sum, a high temperature imposed a negative effect on the CO_2 adsorption on VF–AN–TETA.

Regeneration Performances

Although the regeneration was carried out at 90°C, the regenerative adsorption reached up to 3.93 mmol/g (the fresh adsorption capacity was 4.13 mmol/g), as presented in Figure 8; this was consistent with the fact that the nitrogen content of the regenerated fiber was less than that of the fresh fiber (after 10 regeneration cycles, the nitrogen content of the adsorbent decreased from 17.17 to 15.70%). However, the decrease in the adsorption capacity of VF–AN–TETA after 10 cycles was less than 4%; this

Table IV. Influence of the Temperature on the Adsorption Capacity and Amine Utilization of VF–AN–TETA

Temperature (°C)	Adsorption capacity (mmol/g)	Amine utilization (%)
30	4.3	36.53
40	4.01	33.14
50	3.58	29.58
60	3.07	25.37
70	2.83	23.39
85	1.04	8.06

Fiber mass = 1.0 g; N_2 = 27 mL/min; CO_2 = 3 mL/min.

indicated that the adsorbed CO_2 was totally released under our experimental conditions. This also revealed that VF–AN–TETA retained remarkable stability; this is very important for practical use in industry.

CONCLUSIONS

A solid amine fiber was successfully prepared via the graft copolymerization of AN onto VFs; this was followed by amination with TETA. This VF–AN–TETA was proven to be an excellent adsorbent for CO_2 with a remarkable CO_2 adsorption capacity (4.35 mmol/g), chemical stability, and good regeneration properties. Compared with PP–AN–TETA, the better performance of VF–AN–TETA for CO_2 adsorption could have possibly been related to the higher degree of hydrogen bonding between the carbamate and neighbor hydroxyl groups. This work suggests that VFs will be a novel substrate of CO_2 adsorbents as they have great potential to become economically feasible in CO_2 capture.

ACKNOWLEDGMENTS

The authors gratefully acknowledge the financial support provided by the National Natural Science Foundation of China (contract grant number 51173211) and the Natural Science Foundation of Guangdong Province (contract grant number 2014A030313192).

REFERENCES

1. Schrier, J. *ACS Appl. Mater. Interfaces* **2012**, *4*, 3745.
2. Siriwardane, R. V.; Shen, M. S.; Fisher, E. P.; Poston, J. A. *Energy Fuels* **2001**, *15*, 279.
3. Razavi, S. S.; Hashemianzadeh, S. M.; Karimi, H. *J. Mol. Model.* **2011**, *17*, 1163.
4. Wurzbacher, J. A.; Gebald, C.; Steinfeld, A. *Energy Environ. Sci.* **2011**, *4*, 3584.
5. Zhao, H. L.; Yan, W.; Bian, Z. J.; Hu, J.; Liu, H. L. *Solid State Sci.* **2012**, *14*, 250.
6. Qian, D.; Lei, C.; Hao, G. P.; Li, W. C.; Lu, A. H. *ACS Appl. Mater. Interfaces* **2012**, *4*, 6125.
7. Yu, K.; Kiesling, K.; Schmidt, J. R. *J. Phys. Chem. C* **2012**, *116*, 20480.
8. Liu, Y.; Liu, J.; Chang, M.; Zheng, C. G. *Fuel* **2012**, *95*, 521.
9. Li, W.; Bollini, P.; Didas, S. A.; Choi, S.; Drese, J. H.; Jones, C. W. *ACS Appl. Mater. Interfaces* **2010**, *2*, 3363.
10. Tan, J.; Shao, H. W.; Xu, J. H.; Du, L.; Luo, G. S. *Ind. Eng. Chem. Res.* **2011**, *50*, 3966.
11. Rinker, E. B.; Ashour, S. S.; Sandall, O. C. *Ind. Eng. Chem. Res.* **2000**, *39*, 4346.
12. Yan, X. L.; Zhang, L.; Zhang, Y.; Yang, G. D.; Yan, Z. F. *Ind. Eng. Chem. Res.* **2011**, *50*, 3220.
13. Belmabkhout, Y.; Serna-Guerrero, R.; Sayari, A. *Adsorption* **2011**, *17*, 395.
14. Chen, C.; Son, W. J.; You, K. S.; Ahn, J. W.; Ahn, W. S. *Chem. Eng. J.* **2010**, *161*, 46.
15. Choi, S.; Drese, J. H.; Jones, C. W. *ChemSusChem* **2009**, *2*, 796.
16. Son, W. J.; Choi, J. S.; Ahn, W. S. *Micropor. Mesopor. Mater.* **2008**, *113*, 31.
17. Zhao, A.; Samanta, A.; Sarkar, P.; Gupta, R. *Ind. Eng. Chem. Res.* **2013**, *52*, 6480.
18. Sharma, B. R.; Kumar, V.; Soni, P. L. *J. Appl. Polym. Sci.* **2003**, *90*, 129.
19. Goyal, P.; Kumar, V.; Sharma, P. *J. Appl. Polym. Sci.* **2008**, *108*, 3696.
20. Goyal, P.; Kumar, V.; Sharma, P. *J. Appl. Polym. Sci.* **2009**, *114*, 377.
21. Zu, J. H.; He, S. Q.; Nho, Y. C.; Pyo, J. J.; Yan, F. *J. Appl. Polym. Sci.* **2010**, *116*, 1414.
22. Sayari, A.; Belmabkhout, Y.; Da'na, E. *Langmuir* **2012**, *28*, 4241.
23. Sayari, A.; Belmabkhout, Y. *J. Am. Chem. Soc.* **2010**, *132*, 6312.
24. Su, F. S.; Lu, C. S.; Chen, H. S. *Langmuir* **2011**, *27*, 8090.
25. Yang, Y.; Ma, N. F.; Zhang, Q. K.; Chen, S. X. *J. Appl. Polym. Sci.* **2009**, *113*, 3638.
26. Xu, X. C.; Song, C. S.; Andresen, J. M.; Miller, B. G.; Scaroni, A. W. *Energy Fuels* **2002**, *16*, 1463.
27. Chen, Z. H.; Deng, S. B.; Wei, H. R.; Wang, B.; Huang, J.; Yu, G. *ACS Appl. Mater. Interfaces* **2013**, *5*, 6937.